International Conference on Applied Energy 2019
Aug 12-15, 2019, Västerås, Sweden
Paper ID: 0751

IMPROVED WEIGHTED AVERAGE CURRENT CONTROL OF DUAL-BUCK BIDIRECTIONAL CONVERTER WITH AN LCL FILTER

Feng qiao[1], Qiongbin Lin[1,2*], Shi You[2], Hanmin Cai[2], Yi Zong[2], Chresten Træholt[2]

[1] College of Electrical Engineering and Automation, Fuzhou University

[2] Center for Electric Power and Energy, Technical University of Denmark

ABSTRACT

LCL filters are widely used in microgrid converters because of their high level of harmonic attenuation introduced by series inductors. The main challenge of the LCL filters is to damp the associated resonance peak in order to improve the quality of grid injection current. To address this challenge, this paper presents an improved weighted average current control (WACC) method. It applies grid-voltage-feedforward in an inner loop to solve the resonance peak of the filters and reduce the impacts of the grid voltage harmonics on the grid injection current. A PI controller is designed in an outer loop to keep the DC voltage stable. The improved strategy not only simplifies the design process, but also makes the LCL filter system more robust. Simulation and experimental results verify the feasibility of the proposed strategies applied to a dual-buck bidirectional converter with a LCL filter.

Keywords: Weighted average current control, dual-buck bidirectional converter, LCL filters, PI controller.

1. INTRODUCTION

Recently, distributed generation systems have become a trend to solve energy problems. Distributed power generation can make full use of renewable energy to achieve energy saving and emission reduction, which is an effective supplement to centralized power generation [1]. The bidirectional power capability and flexible regulation characteristics of energy storage systems can improve the acceptance capability of distributed power sources and have broad application prospects [2-3]. In the micro-grid, dual-buck converters, which could achieve a bidirectional power flow, are widely used. With the development of power electronics technology, magnetic components play a very important role in various electronic devices. The tendency of power electronic devices is along with high integration, high frequency and high efficiency.

LCL filters can attenuate high-frequency harmonics and also operate in both stand-alone and grid-connected condition, which are the shortcomings of L filters. However, the filters arise some instability concerns due to their resonance phenomena [4-6]. Authors in [7] propose a method using a splitting capacitor to reduce the order of an LCL system. The zeros and poles of the transfer function are canceled to reduce the filter order by dividing the filter capacitor into two parallel branches according to the ratio of the inductance of both the inverter side and the grid side. However, the inject grid current is sensitive to the grid inductance. Another method is proposed in [8] to reduce the system order by controlling the inductor voltage on the inverter side, which does not need to set multiple resonance compensation links. However, the inject grid current is sensitive to the grid voltage because of its indirect current control. Authors in [9-10] point out that the effect of a capacitive current feedback control is equivalent to paralleling with a virtual resistor on the filter capacitor. A dual-loop control based on the capacitor current feedback has a better performance compared with a single grid current feedback. However, it increases the number of sensors and reduces reliability.

In this paper, we present an improved WACC applied to the LCL dual-buck bidirectional converters. Different from the traditional WACC, the improved WACC increases the grid voltage feedforward link as the inner loop, which can not only reduce the order of the LCL system, but also reduce the influence of grid voltage harmonics. The outer loop is specially designed with a PI controller, which ensures a good dynamic response and eliminates the second ripple of the DC capacitance

Selection and peer-review under responsibility of the scientific committee of the 11th Int. Conf. on Applied Energy (ICAE2019).

voltage when operating in rectification state. Finally, simulation and experimental results verify the effectiveness of the proposed strategy in the bidirectional operating state.

2. SYSTEM DESCRIPTION AND STRATEGY

The topology of an LCL dual-buck bidirectional converter is presented in Fig.1. L_g, L_2, C and L_g, L_1, C form the LCL filter. When it works as an inverter, S_3 is the power frequency switch in the positive half cycle, S_2 is the high frequency switch, D_2 is the freewheeling diode. S_1, S_4 and D_1 work in the negative half cycle. When it works as a rectifier, S_3 and S_4 do not operate. In the positive half cycle, S_1 is a high frequency switching, D_4 is the freewheeling diode. S_2 and D_3 work in the negative half cycle.

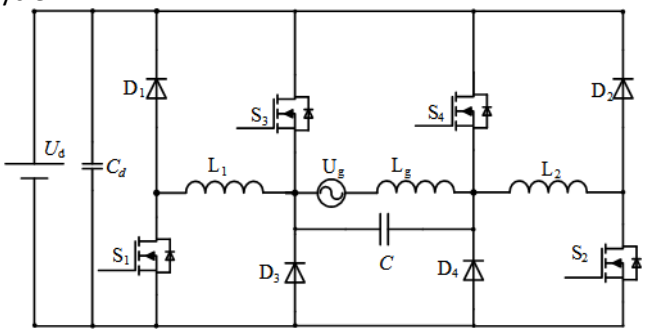

Fig 1 LCL dual-buck bidirectional converter

2.1 Inverter model

The WACC based on grid voltage feedforward is shown in Fig.2, where the weighted sum of the inverter side current and the grid current is used as a comparison in the current loop.

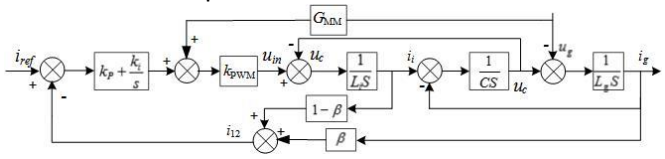

Fig 2 Inverter control block diagram

The transfer functions can be obtained from Fig.2.

$$\begin{cases} G_{u_{in}-i_i}(s)=\dfrac{i_i(s)}{u_{in}(s)}=\dfrac{1+L_gCS^2}{L_iL_gCS^3+(L_i+L_g)S} \\ G_{u_{in}-i_g}(s)=\dfrac{i_g(s)}{u_{in}(s)}=\dfrac{1}{L_iL_gCS^3+(L_i+L_g)S} \end{cases} \quad (1)$$

Set $L=L_i+L_g$, $Li=\alpha L$, then $L_g=(1-\alpha)L$, we have (2) as follows,

$$\begin{cases} G_{u_{in}-i_i}(s)=\dfrac{i_i(s)}{u_{in}(s)}=\dfrac{(1-\alpha)LCS^2+1}{\alpha(1-\alpha)L^2CS^3+LS} \\ G_{u_{in}-i_g}(s)=\dfrac{i_g(s)}{u_{in}(s)}=\dfrac{1}{\alpha(1-\alpha)L^2CS^3+LS} \end{cases} \quad (2)$$

According to Fig.2, we could have $i_{12}=(1-\beta)i_i+\beta i_g$. The transfer function of the feedback current i_{12} to the output voltage of the inverter is shown in (3).

$$G_{u_{in}-i_{12}}(s)=\frac{i_{12}(s)}{u_{inv}(s)}=(1-\beta)G_{u_{in}-i_i}(s)+\beta G_{u_{in}-i_g}(s) \quad (3)$$

$$G_{u_{in}-i_{12}}(s)=\frac{i_{12}(s)}{u_{inv}(s)}=\frac{(1-\beta)(1-\alpha)LCS^2+1}{LS\left[\alpha(1-\alpha)LCS^2+1\right]} \quad (4)$$

With $\alpha+\beta=1$, equation (3) can be rewritten as,

$$G_{u_{in}-i_{12}}(s)=\frac{i_{12}(s)}{u_{inv}(s)}=\frac{1}{LS} \quad (5)$$

From (5), it can be observed that the WACC can reduce the order of the system and that the resonance problem of the LCL filter is solved. Although the LCL filter has a significant attenuation effect on the high-frequency harmonics, the suppression of the background harmonics of the grid is insufficient [11]. So a grid voltage feedforward is added.

Because the capacitor voltage is approximately same as the grid voltage in Fig.1, equations (6) and (7) can be obtained.

$$u_{in}=L_i\frac{di_{iL}}{dt}+u_g \quad (6)$$

$$u_{in}(k)=d(k)u_{dc}(k) \quad (7)$$

where $d(k)$ is the duty cycle. Substituting (7) into (6) and discretizing it result in (8).

$$d(k)=\frac{u_{in}(k)}{u_{dc}(k)}=\frac{(L_i/T_s)\left[i_{iL}(k+1)-i_{iL}(k)\right]+u_g(k)}{u_{dc}(k)} \quad (8)$$

To make the system track the reference current at time step k+1 in the positive half cycle, the current needs to satisfy (9).

$$\begin{cases} i_{iL}(k+1)=i_{ref}(k+1) \\ i_{iL}(k)=(1-\beta)i_{iL}+\beta i_g \end{cases} \quad (9)$$

According to (8) and (9), the parameters of controller can be obtained.

$$\begin{cases} k_P=\dfrac{L_i}{T_sU_d}, k_i=0 \\ G_{MM}=\dfrac{1}{U_d} \end{cases} \quad (10)$$

With the ratio of inductance at the grid and the bridge side, the current feedback β can be obtained.

Thus, the parameters of the PI controller and the grid voltage feedforward are determined.

2.2 Rectifier model

The improved strategy is presented in Fig.3. The WACC based on the grid voltage feedforward as the inner loop can reduce the order of an LCL system and indirectly control the inject grid current to ensure a good level of steady-state performance, while using the PI controller as the outer loop guarantees stability of the DC voltage.

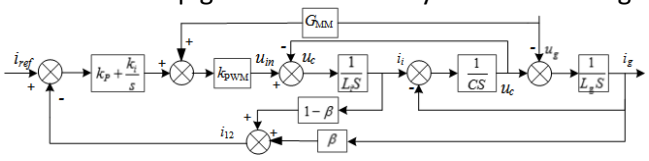

Fig 3 Rectifier control block diagram

The rectifier is equivalent to a boost circuit and this gives (11) and (12).

$$u_g = L_i \frac{di_{iL}}{dt} + u_{rn} \tag{11}$$

$$u_{dc}(k) = \frac{1}{1-d(k)} u_{rn}(k) \tag{12}$$

where u_{rn} is output voltage of the bridge. By discretizing (11), equation (13) could be obtained

$$u_g(k) = \frac{L_i}{T_s}\left[i_{iL}(k+1) - i_{iL}(k)\right] + u_{rn}(k) \tag{13}$$

According to (11) and (12), the duty cycle at time step k can be obtained.

$$d(k) = \frac{(L_i/T_s)\left[i_{iL}(k+1) - i_{iL}(k)\right]}{u_{dc}(k)} + 1 - \frac{u_g(k)}{u_{dc}(k)} \tag{14}$$

The main performance indicators of a voltage loop are stability, accuracy and robustness. Fig.4 shows the voltage loop control block diagram of a rectifier, where $G_{vd}(s)$ is the transfer function of the voltage loop controller, $G_u(s)$ is the transfer function of the voltage loop filter, and $G_w(s)$ is the gain of the PWM rectifier.

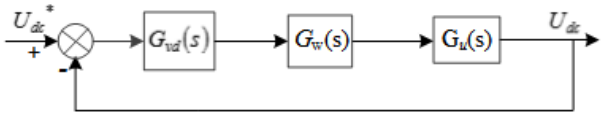

Fig 4 Voltage loop control block diagram

Equation (11) could be rewritten as,

$$u_g(t) = L_i \frac{di_{iL}}{dt} + (1-D)u_{dc} \tag{15}$$

where D is the duty cycle. Set the current equation,

$$(1\text{-}D)i_L = C_d \frac{du_{dc}}{dt} + \frac{u_{dc}}{R} \tag{16}$$

Taking the inductor current $i_L(t)$ and the DC side filter capacitor voltage u_{dc} as state variables, equation (14) can be transformed into

$$\begin{cases} \dfrac{di_L(t)}{dt} = \dfrac{-(1-D)}{L} u_{dc}(t) + \dfrac{u_g(t)}{L} \\ \dfrac{du_{dc}(t)}{dt} = \dfrac{(1-D)i_L(t)}{C_d} - \dfrac{u_{dc}(t)}{RC_d} \end{cases} \tag{17}$$

Adding the disturbance to each state variable in (17) gives,

$$\begin{cases} d = D + \hat{d}, i_{iL}(t) = i_{iL} + \hat{i}_{iL} \\ u_{dc}(t) = u_{dc} + \hat{u}_{dc}, u_g(t) = u_g + \hat{u}_g \end{cases} \tag{18}$$

By substituting (18) into (17), a current loop DC balance equation of the boost circuit can be obtained. Then the small signal is linearized by eliminating the large signal and the high-order small signal.

$$\frac{d\hat{i}_{iL}}{dt} = \frac{\hat{u}_g}{L_i} - \frac{1\text{-}D}{L_i}\hat{u}_{dc} + \frac{\hat{d}}{L_i}u_{dc} \tag{19}$$

The same method can be used to obtain a DC balance equation of the voltage loop, and its small signal linearization equation is,

$$u_{dc}(s) = \hat{i}_{iL}(s)\frac{(1-D)R}{RC_dS+1} - \frac{u_{dc}}{(1-D)(RC_dS+1)}\hat{d}(s) \tag{20}$$

By substituting (20) into (19)

$$\begin{aligned} (RC_dS+1)S\hat{i}_{iL}(s) &= \frac{u_{dc}}{L_i}\hat{d}(s) - \frac{(1\text{-}D)^2 R}{L_i}\hat{i}_L(s) \\ &+ \frac{u_{dc}(RCs+1)}{L_i}\hat{d}(s) + \frac{\hat{u}_g}{L_i} \end{aligned} \tag{21}$$

Neglecting the disturbance of the grid, the transfer function of the duty cycle to the grid current, the duty cycle to the DC voltage, and the grid current to the DC voltage could be obtained as follows.

$$G_{id}(s) = \frac{i_g(s)}{d(s)} = \frac{u_{dc}(2+RC_dS)}{RLCS^2 + L_iS + (1\text{-}D)^2 R} \tag{22}$$

$$G_{vd}(s) = \frac{u_{dc}(s)}{d(s)} = \frac{\left[(1-D)R - SL_i/(1-D)\right]}{RLCS^2 + L_is + (1-D)^2 R} \tag{23}$$

$$G_{vi}(s) = \frac{u_{dc}(s)}{i_g(s)} = \frac{(1\text{-}D)R - L_iS/(1-D)}{2+RCS} \tag{24}$$

The open loop transfer function with the PI controller is,

$$G_u(s) = G_{vd}(s)G_{vi}(s) = \frac{u_g{}^2R - u_{dc}{}^2L_iS}{u_g u_{dc}(2+RCS)}\left(k_p + \frac{k_i}{s}\right) \tag{25}$$

Therefore, the zero point of the PI controller is set at the crossing frequency. In addition, in order to suppress

the secondary ripple in the capacitor voltage, the crossing frequency is set to 1/10 times the secondary ripple frequency i.e. $f_c=f_z=10Hz$. Since the gain at the crossing frequency is 1, the zero frequency of the PI controller is approximately the crossing frequency.

$$\begin{cases} |G_i(j2\pi f_c)|=1 \\ \dfrac{k_i}{k_p}=2\pi f_z \end{cases} \tag{26}$$

From the formula above, the parameters are determined as k_p = 0.052 and k_i = 3.267. A Bode diagram of the open-loop transfer function is shown in Fig.5. The phase margin is 59°, which indicates the system is stable. The amplitude attenuation of 100 Hz is about -23dB, which implies the secondary ripple of the DC voltage is sufficiently suppressed.

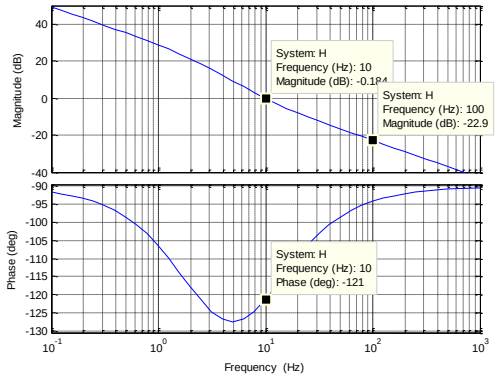

Fig 5 The Bode diagrams of voltage loop

3. SIMULATION

In order to verify the effectiveness of the proposed strategy, the PSIM is used to build the circuit. The simulation parameters are listed in Table 1.

Table 1 LCL dual-buck converter parameters

Parameter	*Value*
Grid voltage/ *V*	220
DC voltage/ *V*	360
DC capacitive/ *uF*	1000
Grid side inductor/ *mH*	1
Bridge side inductor/ *mH*	0.4
Capacitive of filter/ *uF*	2.2
Grid frequency/ *Hz*	50
Switching frequency/ *kHz*	20
Power/ *W*	1000

The simulation results of the inverter are shown in Fig.6, which proves the effectiveness of the proposed strategy. At full load, the distortion of inject grid current is calculated to be THD=2.29%, and there is no distortion problem caused by delay near the zero-crossing point. This indicates that the inject grid current satisfies existing standard and it has high quality. Fig.7 shows the change of the grid current from half load to full load of the rectifier in 0.12s, which means the system has an acceptable dynamic performance.

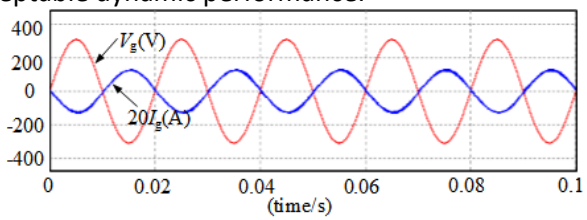

Fig 6 The simulation result at AC-DC

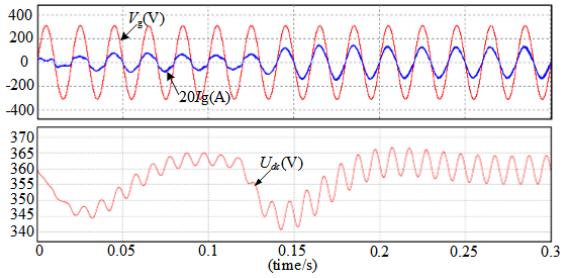

Fig 7 The simulation result at DC-AC

4. EXPERIMENT

A 1000W prototype was built to verify the effectiveness of the proposed strategy as shown in Fig.8. Parameters of the prototype are listed in Table 1. The converter is controlled by a digital chip TMS320F28377D from Texas Instruments.

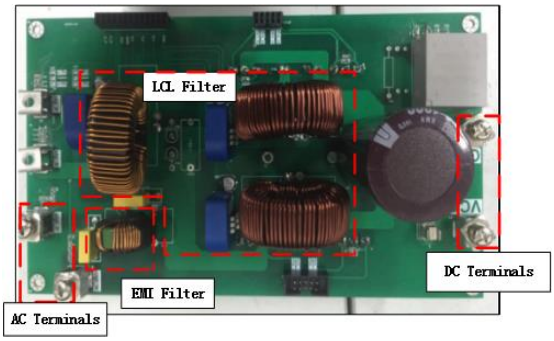

Fig 8 Experimental prototype

The inject grid current of the LCL dual-buck converter working as a grid-connected inverter is shown in Fig.9. Fig.9(a) and (b) show quality of the inject grid current at 1000W and 500W, respectively. The waveforms of the rectifier are shown in Fig.10. Fig.10(a) and (b) show waveforms at 1000W and 500W, respectively. The THD of grid current and PF are listed in Table 2.

Table 2 Experiment results

Mode	Power/W	THD/%	PF
Inverter	1000	3.29	0.996
	500	3.78	0.995
Rectifier	1000	3.73	0.997
	500	5.3	0.996

The experimental results show that the proposed strategy can effectively address the resonance problem and enhance the stability of the system. The THD of the inject grid current and the power factor can satisfy the design requirements.

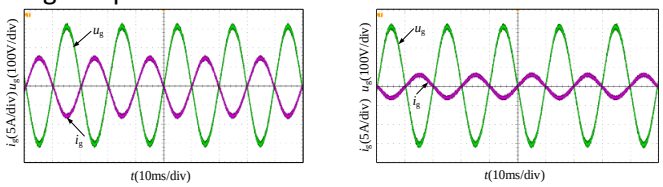

(a) P=1000W (b) P=500W

Fig 9 The inject grid current at DC-AC

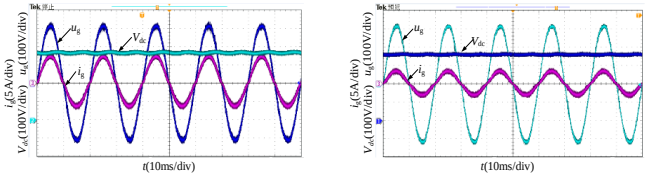

(a) P=1000W (b) P=500W

Fig 10 The experimental waveforms at AC-DC

5. CONCLUSION

In this paper, a dual-buck bidirectional converter with smaller volumes and better inject grid current by using LCL filters was designed. In the inverter mode, the WACC based on grid voltage feedforward was used to reduce the resonance peak of the filter. The grid voltage feedforward could effectively suppress the grid disturbance and reduce the impacts of the grid voltage harmonic on the inject grid current, which improves the gird current quality. In the rectifier mode, an improved voltage and current dual-loop control was proposed. The inner loop reduced the order of the LCL filter and the indirect control of the grid current through the WACC based on the grid voltage ensured the grid current quality. A PI controller as outer loop kept the output DC voltage stable. The experimental results of a 1000W prototype demonstrated the effectiveness of the proposed method.

ACKNOWLEDGEMENT

This work was supported in part by the Technology Innovation Fund Support Project by the company of Kehua Hengsheng under Grant KHHS20170416.

REFERENCE

[1] Ehsan A, Yang Q. Optimal integration and planning of renewable distributed generation in the power distribution networks: A review of analytical techniques[J]. Applied Energy, 2018, 210: 44-59.

[2] Rostampour V, Jaxa-Rozen M, Bloemendal M, et al. Aquifer Thermal Energy Storage (ATES) smart grids: Large-scale seasonal energy storage as a distributed energy management solution[J]. Applied Energy, 2019, 242: 624-639.

[3] Chen W, Zeng Y, Xu C. Energy storage subsidy estimation for microgrid: A real option game-theoretic approach[J]. Applied Energy, 2019, 239: 373-382.

[4] Wu W, He Y, Tang T, et al. A New Design Method for the Passive Damped LCL and LLCL Filter-Based Single-Phase Grid-Tied Inverter[J]. IEEE Transactions on Industrial Electronics, 2013, 60(10):4339-4350.

[5] Dannehl J , Liserre M , Fuchs F W . Filter-Based Active Damping of Voltage Source Converters With Filter[J]. IEEE Transactions on Industrial Electronics, 2011, 58(8):3623-3633.

[6] Gomes C C, Cupertino A F, Pereira H A. Damping techniques for grid-connected voltage source converters based on LCL filter: An overview[J]. Renewable and Sustainable Energy Reviews, 2018, 81: 116-135.

[7] Shen G , Xu D , Cao L , et al. An Improved Control Strategy for Grid-Connected Voltage Source Inverters with an LCL Filter[J]. IEEE Transactions on Power Electronics, 2008, 23(4):1899-1906.

[8] Chen Y, Xie Z, Zhou L, et al. Optimized design method for grid-current-feedback active damping to improve dynamic characteristic of LCL-type grid-connected inverter[J]. International Journal of Electrical Power & Energy Systems, 2018, 100: 19-28.

[9] Yoon S , Kwon J , Park J , et al. Indirect Current Control for Seamless Transfer of Three-Phase Utility Interactive Inverters[C]// Applied Power Electronics Conference and Exposition (APEC), 2011 Twenty-Sixth Annual IEEE.2011.

[10] He J , Li Y W . Generalized Closed-Loop Control Schemes with Embedded Virtual Impedances for Voltage Source Converters with LC or LCL Filters[J]. IEEE Transactions on Power Electronics, 2012, 27(4):0-1861.

[11] Jalili K , Bernet S . Design of Filters of Active-Front-End Two-Level Voltage-Source Converters[J]. IEEE Transactions on Industrial Electronics, 2009, 56(5):1674-1689.